



# The influence of particle morphology on microbially induced CaCO<sub>3</sub> clogging in granular media

Chenpeng Song<sup>a,b</sup>, Derek Elsworth<sup>b</sup>, Sheng Zhi<sup>b</sup> and Chaoyi Wang<sup>b</sup>

<sup>a</sup>National and Local Joint Engineering Laboratory of Traffic Civil Engineering Materials, Chongqing Jiaotong University, Chongqing, China;

<sup>b</sup>Department of Energy and Mineral Engineering, EMS Energy Institute and G3 Center, Pennsylvania State University, University Park, PA, USA

## ABSTRACT

*Sporosarcina pasteurii* (ATCC 11859) is a nitrogen-circulating bacterium capable of precipitating calcium carbonate given a calcium source and urea. This microbially induced carbonate precipitation (MICP) is able to infill inter-granular porosity and act as a biological clogging agent, thus having a wide potential application in strengthening coastal foundations, preventing erosion by seas and rivers and in reducing sand liquefaction potential in coastal areas. A successful MICP application requires the understanding of the primary parameters that influence the microbially mediated process to achieve its engineering goals, such as injection scheme, chemical concentrations, retention times, and injection rates. However, the granular morphology has generally been oversimplified to ideal shape without enough consideration in previous studies. The following explores the critical micro-scale influence of particle morphology on mechanisms of microbially induced clogging. Spherical, non-spherical and angular particles were used as granular aggregates in permeating column experiments with the resulting permeability and calcium carbonate content of the treated aggregates examined. Microscopic examination (SEM) defines the features of the distribution of microbially precipitated calcium carbonate and the forms of clogging. The results show: (1) given a fixed duration of treatment, the calcium carbonate content for the spherical particle aggregate is significantly higher than that for near-spherical and angular particle aggregates; (2) for identical durations of treatment, the maximum permeability reduction occurs for angular particles (rather than for spherical particles with the highest carbonate content). This suggests that the microscopic distribution of calcium carbonate is significantly influenced by particle morphology, exerting a critical control in the effectiveness of clogging. SEM images indicate that the microbial calcium carbonate precipitates encapsulate the spherical particles as a near-uniform shell and occlude the pore space only by increasing the shell thickness. In contrast, the near-spherical and angular particles are only partially coated by a calcium carbonate film with scattered crystals of vaterite and calcite further clogging the void space. The polyhedral nature of the non-spherical particles tends to result in a slot-shaped pore structure which critically defines the hydraulic conductivity of the ensemble medium. As the microbial vaterite and calcite continue to accumulate on the particle surface, these slot-shaped pore structures become increasingly more tortuous – resulting in a noticeable reduction of permeability at a lower calcium carbonate content.

## ARTICLE HISTORY

Received 15 June 2019

Accepted 14 September 2019

## KEYWORDS

Microbially induced clogging; *Sporosarcina pasteurii*; particle morphology; microbial calcium carbonate; permeability; granular media

## 1. Introduction

Biom mineralization is caused by cell-mediated phenomena and is the process by which living organisms produce minerals in nature (Hu, Liu, and Ma 2011; Weiner 2005). Microbially induced carbonate precipitation (MICP) is a common form of biom mineralization. The main groups of microorganisms that can induce carbonate precipitation include cyanobacteria and microalgae, sulfate-reducing bacteria, and some species of microorganisms involved in the nitrogen cycle (Ariyanti, Abyor, and Hadi 2011). *Sporosarcina pasteurii* (ATCC 11859) is a nitrogen-circulating gram-positive bacterium that is most commonly employed for MICP (Song and Elsworth 2018; van Paassen

2009). *Sporosarcina pasteurii* can continually produce highly active urease in its metabolic process. This enzyme is able to catalyze the hydrolysis of urea into ammonium and carbonate. When this hydrolysis occurs in a calcium-rich environment, the carbonate generated from the hydrolysis will form calcium carbonate precipitate, which then envelops the bacterium (DeJong, Fritzges, and Nüsslein 2006; Rebata-Landa 2007). Thus, the bacteria also act as nucleation sites for the calcium carbonate.

This form of MICP may both cement the soil matrix and fill the pore space and thus is able to act as a biological clogging agent that both strengthens the porous medium and reduces its permeability. In particular, the MICP in granular

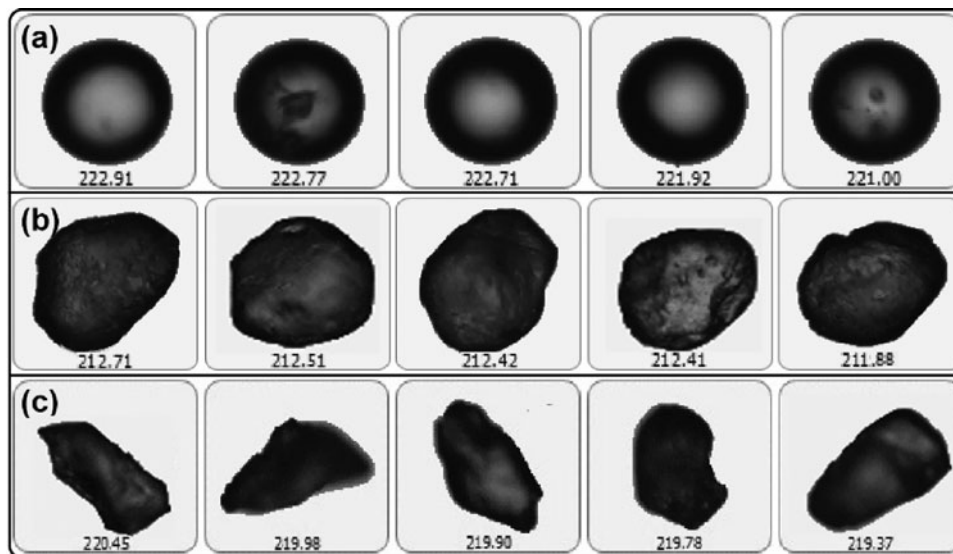


**Figure 1.** Typical 2D projections of the three sample categories showing estimated particle diameters ( $\mu\text{m}$ ) (i.e. largest width, as displayed under each image): (a) artificial silica sand (spherical particle shape), (b) Ottawa sand (polyhedral particle shape), (c) crushed Ottawa sand (angular particle shape).

medium has been studied widely for beneficial uses in eco-friendly construction materials, groundwater control, and environmental remediation (Phillips et al. 2013; Qian, Wang, and Wang 2015; van Paassen et al. 2010). MICP can also be applied in marine geotechnical applications such as the strengthening of coastal foundation, preventing erosion by seas and rivers and in reducing sand liquefaction potential in coastal areas (Khodadadi Tirkolaei and Bilsel 2017; Liang et al. 2019; Tian et al. 2019; Wang et al. 2017). A successful MICP application requires the understanding of the primary parameters that influence biomineralization to achieve its engineering goal. The concentrations of the biochemical reactants (bacteria, urea, and  $\text{Ca}^{2+}$ ), the injection rate of the solution, the injection scheme, and fluid residence time (Al Qabany, Soga, and Santamarina 2012; Baveye et al. 1998; Qabany and Soga 2013) have been extensively studied as the primary influential factors for MICP. However, the granular morphology has generally been oversimplified to ideal shape without enough consideration. Previous studies have used Ottawa sand as a standard permeable aggregate to allow cross-comparisons of the effectiveness of MICP treatment, while Ottawa sand is a naturally occurring near-spherical near-pure quartz sand from the St. Peter formation (Erdoğan et al. 2017). When it comes to specific sand-cementing problem, the use of Ottawa sands makes it an ideal and logical aggregate to study the influence of controlling MICP clogging. However, when it comes to a broader utilization of MICP, the characteristics of shapes of granular porous media become variant. Besides the near-spherical shape, the granular porous media may also comprise angular and sub-angular particles that alter packing and surface characteristics. Understanding the effects of particle morphology on the microscopic response to MICP-precipitation and clogging and its macroscale impact on permeability is the focus of this study.

The following explores the microscale characteristics of MICP-clogging and its impact on macroscale seepage behavior by preparing mineralogically identical quartz sands of

different angularities. Artificial silica sand (spherical particles), Ottawa sand (near-spherical particles) and crushed Ottawa sand (angular particles) are used as variable modally compositional aggregates to examine the mechanisms and impacts of microbial clogging for different durations.

## 2. Materials and methods

We explore the effectiveness of microbially induced clogging by preparing mineralogically identical quartz sands of various angularities. These contrasting control samples are then treated by the application of MICP for different durations and the levels of permeability change measured.

### 2.1. Particle types and characterizations

Three types of quartz particles are used as aggregates for MICP treatment, representing spherical particles (artificial silica sand), near-spherical particles (intact Ottawa sand) and angular particles (crushed Ottawa sand). The particle size of all particle shape categories is uniform at 60–80 mesh (0.25–0.18 mm). We characterize the three distinct morphologic categories using a Morphologi G3 analyzer to define particle shape distributions. The typical morphologic images of these three categories of aggregates are shown in Figure 1. The distribution and median value of particle circularity for the three sample classes are shown in Figure 2 and Table 1. The artificial silica sand features the highest circularity followed by Ottawa sand and crushed Ottawa sand. Circularity is a measure of the closeness to a circle and is sensitive to both changes in overall form and edge roughness (Nouri and Sola 2018). Figure 3 shows the circularity value of some example shapes. All the prepared aggregates are soaked in a solution of hydrochloric acid (5 mol/L) for 12 h and are then washed with deionized water and dried at  $105^\circ\text{C}$  for 24 h prior to use.

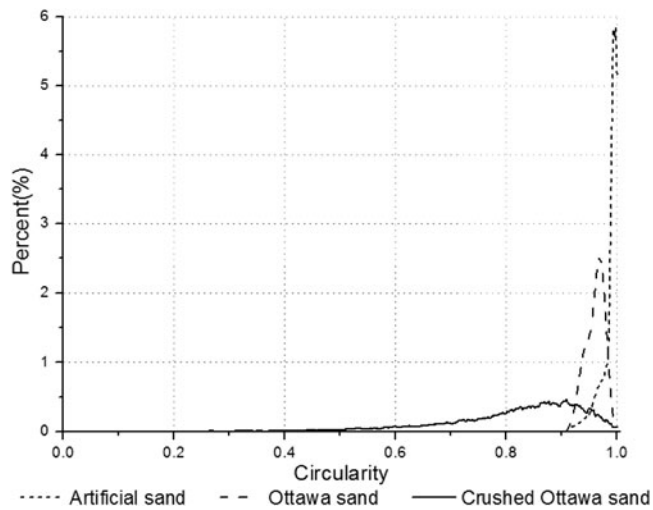


Figure 2. Circularity statistical distribution of three types of sand.

Table 1. Median circularity values of particles.

Artificial silica sand	Ottawa sand	Crushed Ottawa sand
0.992	0.956	0.841

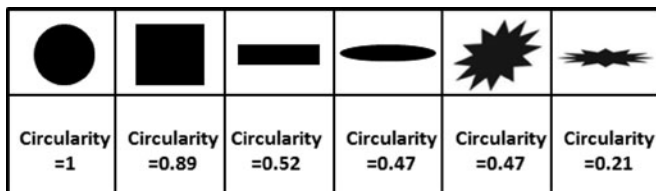


Figure 3. The circularity value of some familiar shapes.

## 2.2. Bacteria cultivation

*Sporosarcina pasteurii* is obtained from the American Type Culture Collection (freeze-dried, ATCC 11859). The growth medium is NH<sub>4</sub>-YE (ATCC 1376, Table 2). The activated bacteria are cultured at 30 °C in a shaking water bath (200 r/min) for 36–48 h, reaching the late exponential/early stationary phase of evolution, and are harvested at OD<sub>600</sub> = 1.4 [OD<sub>600</sub> is the optical density at a wavelength of 600 nm and is used as an indication of biomass concentration (Sutton 2011)]. The bacterial solution culture is centrifuged at 4000 g for 30 min, the supernatant fluid removed and supplemented by the NH<sub>4</sub>-YE growth medium. After repeating the centrifugal process once, the bacteria solution is stored at 4 °C prior to use.

## 2.3. Column bead-pack flow assembly and experimental procedure

A cylindrical PVC tube [1-inch (25 mm) in inner diameter and 14-inch (350 mm) in length] is used as the experimental core holder with the sand column 10-inch (250 mm) in length. The initial porosity and initial permeability of the columns are shown in Table 3. The results indicate that initial porosity generally increases slightly and initial permeability decreases significantly as the particle shape becomes angular. This is because the polyhedral shape of the crushed sand particles results in significant differences in

Table 2. Ingredients of ammonium-yeast extract medium ATCC 1376.

Yeast extract	20.0 g
(NH <sub>4</sub> ) <sub>2</sub> SO <sub>4</sub>	10.0 g
0.13 M Tris buffer (PH 9.0)	1.0 L
Agar	20.0 g

Table 3. The initial porosity and initial permeability of each type of aggregate.

Initial parameters	Artificial silica sand	Ottawa sand	Crushed Ottawa sand
Porosity (%)	38.5	39.7	40.1
Permeability $k_0$ (Darcy)	4.72	2.50	1.12

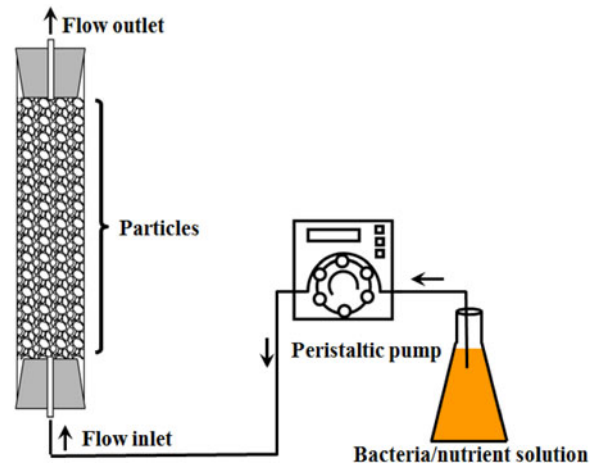


Figure 4. Schematic of the experimental facility.

distributions of intergranular pore-size and morphology. This in turn yields narrow pore throats whose connectivity, size and morphology crucially control the permeability of the ensemble medium. The experimental facility is shown in Figure 4. The bacterial solution and nutrient solution are injected into the column via a peristaltic pump connected to the bottom inlet of the core holder. The fluid injection is one-way – simulating the transport of bacteria/nutrients in the granular medium. Cementation is accomplished by the staged introduction of bacterial solution, stabilizing fluid and the nutrient solution into the sample. The procedure is as follows:

- The bacterial liquid is injected into the sample at a rate of 0.5 mL/min for 60 min (total of 30 mL).
- Injection is halted and the sample left for 2 h for the bacteria to be absorbed to the surfaces of the particles.
- Stabilizing solution is injected into the sample at 0.5 mL/min for 20 min (total of 10 mL). The stabilizing solution is 0.05 mol/L calcium chloride and can stimulate the immobilization and flocculation of bacteria that have adhered to the surfaces of particles (Al Qabany, Soga, and Santamarina 2012; Harkes et al. 2010; van Paassen et al. 2010).
- The final step is injecting the cementing fluid at 0.25 mL/min for 400 min (total of 100 mL). This solution comprises 1.0 mol/L calcium chloride and 1.0 mol/L urea.

Procedures a–d constitute a single full injection cycle. The sand flow-through columns for all three categories of particle shape are individually performed to 4, 6 and 8 cycles of injection to represent different treatment durations.

### 3. Experimental results

After MICP treatment, each column is dissected longitudinally into five equal-length segments [2-inch (50 mm) in length] to measure both permeability and calcium carbonate content of each section. The permeability is measured based on Darcy's law (Wu et al. 2017),

$$k = \frac{QL\mu}{\Delta p A} \quad (1)$$

where  $k$  is the permeability,  $Q$  is the volumetric flow rate,  $\mu$  is the dynamic viscosity of the fluid,  $L$  is the length of the specimen,  $\Delta P$  is the pressure difference, and  $A$  is the cross-sectional area of the sample.

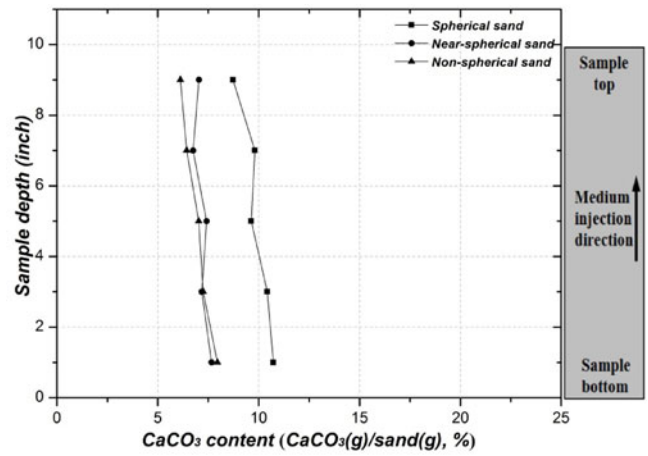
The calcium carbonate ( $\text{CaCO}_3$ ) content is examined by immersing a part of each sample into 5.0 mol/L hydrochloric acid to fully remove the carbonate and then measuring mass difference before and after this treatment. The formula of calcium carbonate content is as follows,

$$W_{\text{CaCO}_3} = \frac{M_{\text{sand}+\text{CaCO}_3} - M_{\text{sand}}}{M_{\text{sand}}} \quad (2)$$

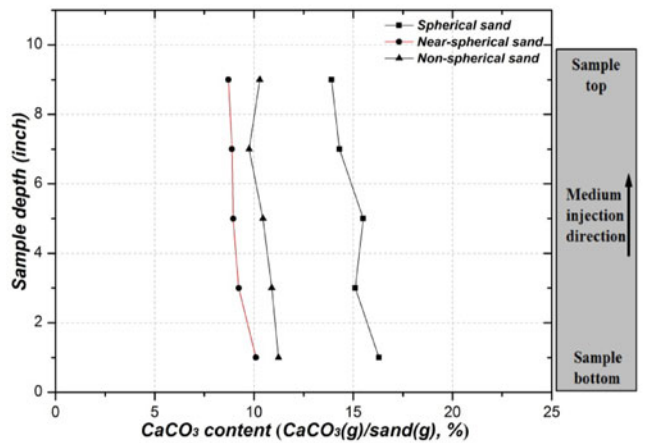
where  $W_{\text{CaCO}_3}$  is the calcium carbonate content,  $M_{\text{sand}+\text{CaCO}_3}$  and  $M_{\text{sand}}$  represent the dry weight of the sample before and after immersing in hydrochloric acid, respectively.

The change in calcium carbonate content with the increased treatment duration is shown in Figure 5. Overall, the  $\text{CaCO}_3$  content for all granules of the aggregates increases with increased nutrient injection volume. Moreover, as the distance of nutrient transport increases, the distribution of  $\text{CaCO}_3$  in the column is not significantly different – presumably due to the high initial concentration of the nutrient solution and the relatively short length of the column. Notably, the  $\text{CaCO}_3$  content of the artificial silica sand (spherical) is significantly larger than the intact and crushed Ottawa sand for the same duration treatment.

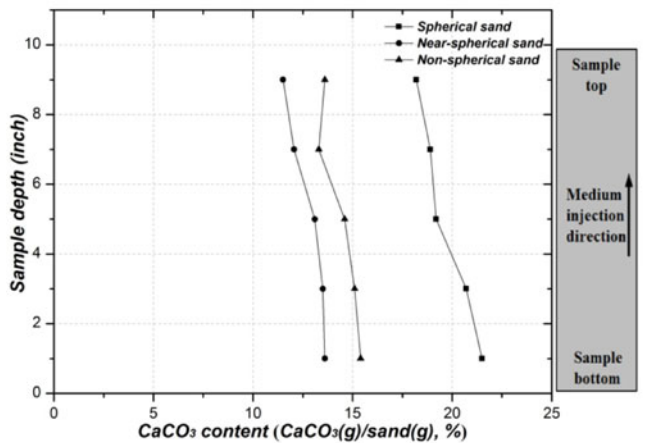
Measured permeabilities are shown in Figure 6. The dimensionless relative permeability ( $k/k_0$ ) is used to compare the normalized effectiveness of clogging among these three categories of aggregates, where  $k_0$  represents the initial permeability of the untreated aggregates. Although spherical particles gain a higher calcium carbonate content compared with the other two, this does not automatically return a higher drop in permeability. Specifically, after 8 cycles of injection, the maximum  $\text{CaCO}_3$  content for the spherical particles (artificial silica sand) has reached 21.5% (at the inlet) and its permeability has only dropped to 48% of its initial permeability ( $k/k_0 = 0.48$ ). By comparison, the non-spherical particles (crushed Ottawa sand) return the maximum drop in permeability ( $k/k_0 = 0.11$ ), although  $\text{CaCO}_3$  content is only 15.4%. The correspondence between calcium carbonate content and the change in permeability for these three categories of particles is shown in Figure 7. In terms



(a) Calcium carbonate content after 4 injection cycles.



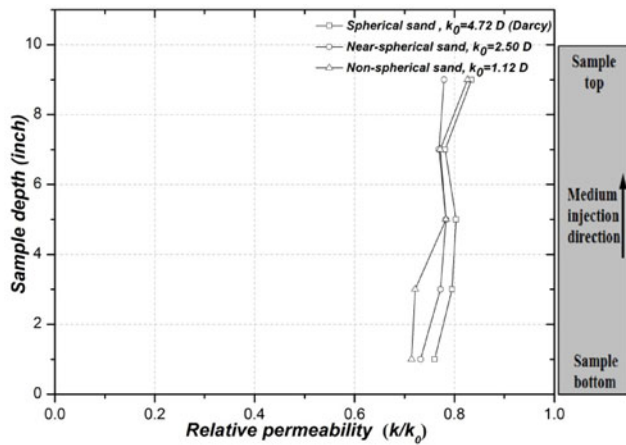
(b) Calcium carbonate content after 6 injection cycles.



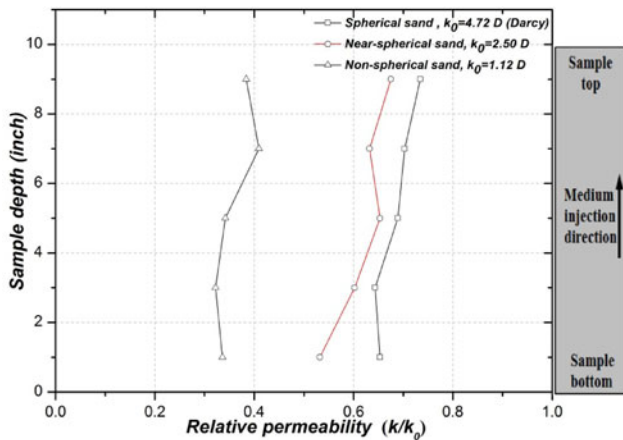
(c) Calcium carbonate content after 8 injection cycles.

Figure 5. Variation in calcium carbonate content with an increased number of microbial injection cycles.

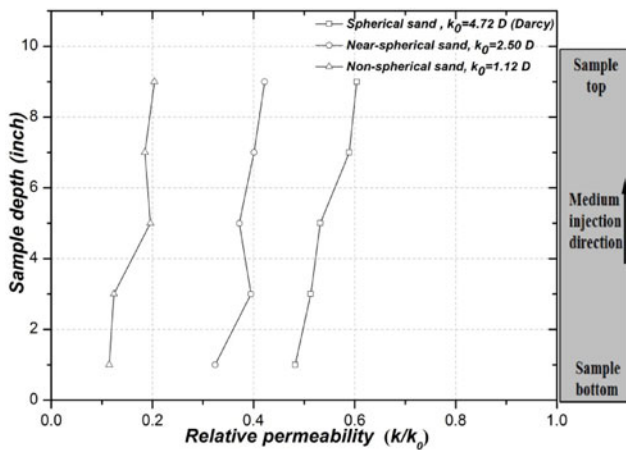
of clogging efficiency, the angular grains undergo the highest permeability reduction followed by the near-spherical particles with the spherical particles the least. The apparent anomaly between the  $\text{CaCO}_3$  content and permeability is explained by examining the microscopic patterns of the clogging in the interstitial space, discussed in the following section.



(a) The permeability after 4 injection cycles.



(b) The permeability after 6 injection cycles.



(c) The permeability after 8 injection cycles.

**Figure 6.** Variation of normalized permeability ( $k/k_0$ ) with an increased number of microbial injection cycles.

#### 4. Microscopic analysis and discussion

We determine the mineralogy of the generated calcium carbonate by X-ray diffraction (XRD) using the powdered substrates. Scanning electron microscopy (SEM) is used to analyze the microstructure of the precipitated calcium

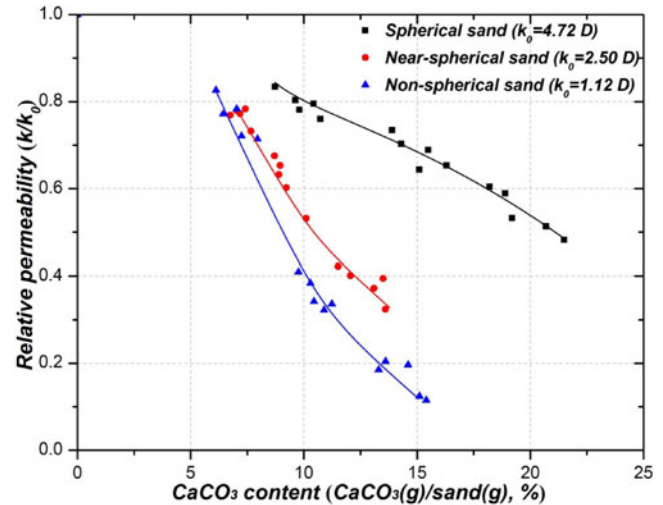


**Figure 7.** Correlation between calcium carbonate content and relative permeability.

carbonate together with its distribution within the intergranular spaces.

#### 4.1. Crystal structure and pore-scale distribution of microbially induced calcium carbonate

The specimens with 6 cycles of biotreatment are used for XRD analysis and SEM. As shown in Figure 8, the mineral forms of the generated calcium carbonate include vaterite and calcite. Among them, vaterite accounts for more than 90% of all these three specimens. Quartz is the mineral component representing the Ottawa sand. Spherical silica sand is amorphous, so no quartz is detected.

For the spherical artificial silica sand (Figure 8(a)), the precipitated calcium carbonate forms a nearly homogeneous shell which uniformly coats the particle surface. This likely results from an initially uniform distribution of the microbes on the particle surface which helps facilitate the uniform precipitation. As the  $\text{CaCO}_3$  shell grows in thickness, the pore spaces reduce. The features of the generated calcium carbonate on the particle surfaces of both intact Ottawa sand (near-spherical) and crushed Ottawa sand (angular) are similar, as shown in Figure 8(b,c), respectively. The particle surfaces are only partially enveloped by thin layers of calcium carbonate with irregularly distributed vaterite and calcite crystals generated on the surfaces.

Previous studies indicated that the morphology of the bacteria affects their adhesion to different roughness of surfaces (Whitehead et al. 2006; Whitehead and Verran 2006). Spheroidal bacteria strongly adhere to rough surfaces, whereas rod-shaped bacteria adhere more firmly to smooth surfaces. This phenomenon is due to the small contact area between the rod-shaped bacteria and the rough surface, resulting in limited binding energy, which may be washed out from the surfaces. Spherical bacteria are smaller in size and easier to insert into surface grooves, so they adhere more firmly to rough surfaces. Figure 9 shows, schematically, the attachment of both rod-shaped and spherical

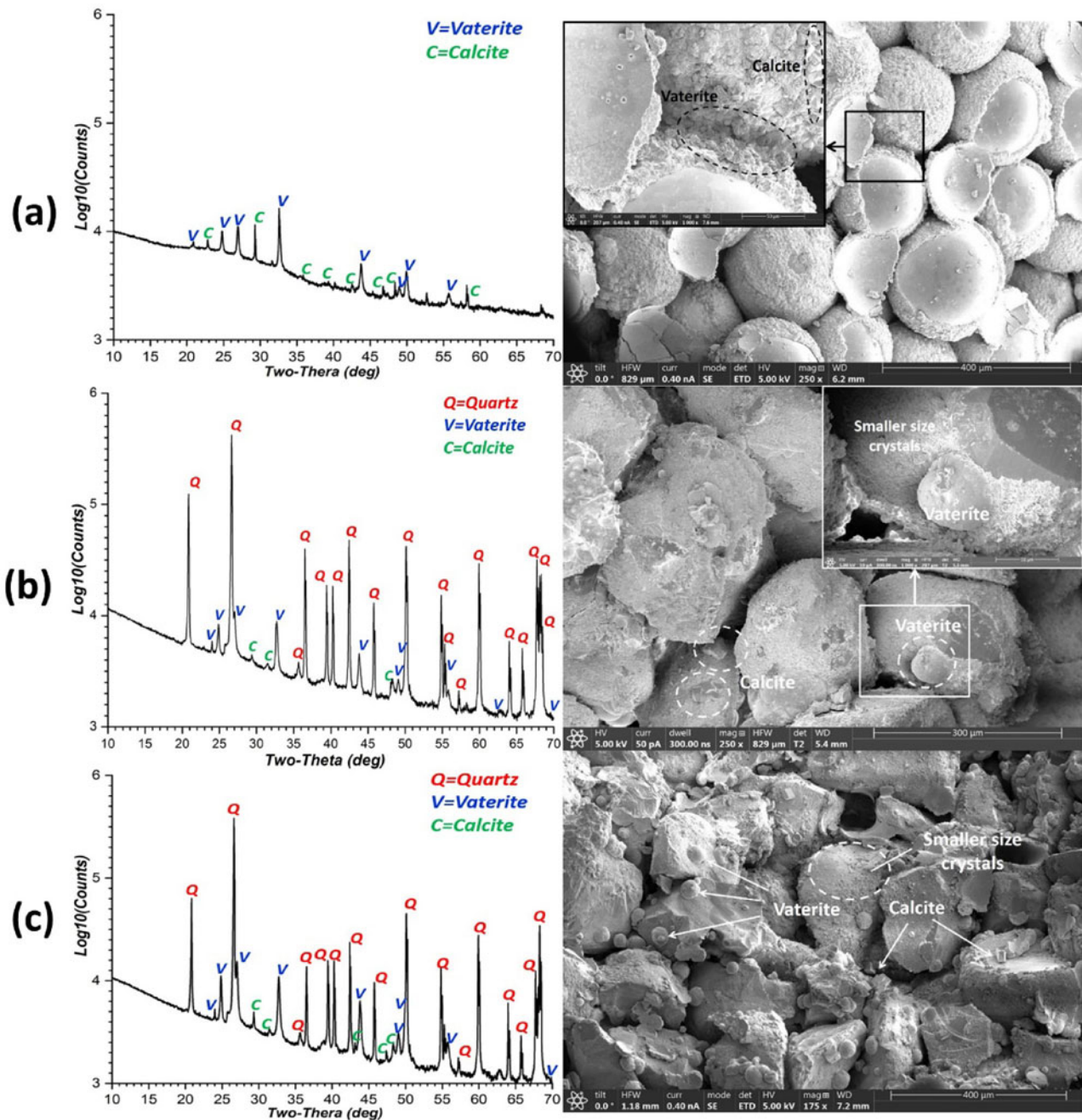


**Figure 8.** XRD analysis and SEM images of these three types of particle aggregates after 6 cycles of biotreatment, (a) spherical particles, (b) near-spherical particles, (c) angular particles.

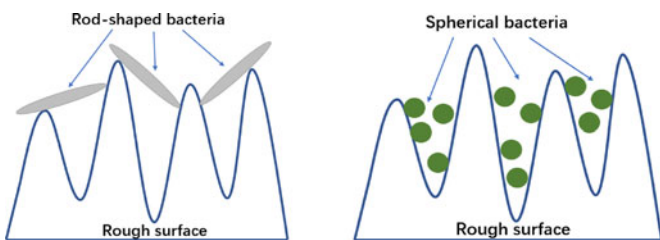


**Figure 9.** Schematic diagram representing the attachment of rod-shaped and spherical bacteria to rough surfaces.

bacteria to rough surfaces. *Sporosarcina pasteurii* is a rod-shaped bacterium, and the surface of artificial silica sand particle is much smoother than those of the intact and crushed Ottawa sand. Thus, the bacteria adhere more readily

and forcefully to the artificial silica sand surfaces and consequently produce more attached and homogeneous calcium carbonate.

#### 4.2. The mechanism of clogging

The morphologies of the interparticle space and the precipitation patterns of calcium carbonate together determine the effectiveness of microbially induced clogging. Although spherical particles (artificial silica sand) can accommodate a larger mass of calcium carbonate by developing a uniform covering of the particle surface, this precipitation pattern does not guarantee a better effectiveness in clogging. As shown in Figure 8(a), although the pore space clearly

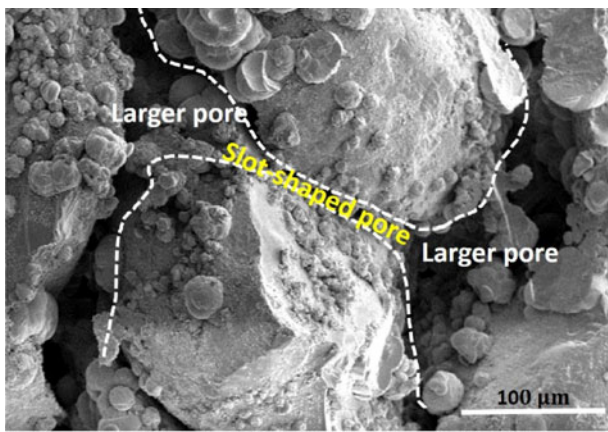


**Figure 10.** Interstitial morphology of irregular particle aggregates.

shrinks following microbial treatment, the degree of pore connectivity is not qualitatively changed. As the particle morphology becomes irregular, the larger intergranular pores tend to be connected by slot-shaped pores, whose connectivity crucially controls the permeability of the ensemble medium (Figure 10). With microbially derived vaterite and calcite gradually accumulating on the particle surface, the connection between these slot-shaped pore channels become progressively more tortuous, thus resulting in an obvious decrease in pore connectivity and permeability. This microscopic distinction explains why the effectiveness of calcium carbonate precipitation on non-spherical particles media shows the highest reduction in permeability, and that for spherical particles, the lowest. The ensemble permeability of the clogged sample is crucially related to the microscopic precipitated form of calcium carbonate and the interstitial morphology.

## 5. Conclusions

We explored the macroscopic and microscopic features of microbially induced clogging in quartz sand aggregates comprising various particle morphologies. The contrasting particle morphologies are spherical (artificial silica sand), near-spherical (Ottawa sand) and angular (crushed Ottawa sand). With different durations of exposure to precipitation/cementation, the generated calcium carbonate contents, resultant alteration in permeability, and SEM images are used together to define controls on microbially induced clogging within the pore space. Amongst these variables, particle shape is shown to exert a major control on the effectiveness and patterns of clogging. The following conclusions are drawn:

- Sporosarcina pasteurii* adheres more readily and forcefully to the surfaces of the smoother particles (spherical particles) and consequently attach a greater mass and more homogeneous distribution of calcium carbonate than more angular particles. Therefore, given a fixed duration of treatment, spherical particles (artificial silica sand) accumulate a larger mass of calcium carbonate compared to both the near-spherical (intact Ottawa

sand) and non-spherical (crushed Ottawa sand) particles.

- However, the higher calcium carbonate contents resulting for the spherical particle aggregates do not result in more-complete clogging – suggesting that the microscopic distribution of microbial calcium carbonate is significantly different among various morphologies of particles and exerts a critical control in the effectiveness of clogging.
- The polyhedral nature of the non-spherical particles generates a slot-shaped pore structure following precipitation which critically determines the ensemble permeability of the granular pack. As microbially precipitated vaterite and calcite continuously accumulate on the particle surface, the slot-shaped pore structure becomes increasingly more tortuous – resulting in a greater reduction in permeability at a lower calcium carbonate content.

Importantly, particle morphology is a key variable in defining the effectiveness of microbial clogging that significantly affects the pattern of precipitation of  $\text{CaCO}_3$ , interstitial morphology, the form of clogging and, as a result, the ensemble permeability of the granular media.

## Disclosure statement

We declare that we do not have any commercial or associative interest that represents a conflict of interest in connection with the work submitted.

## Funding

This paper is a result of support from the National Science Foundation of China (No. 51604051), the Natural Science Foundation of Chongqing (No. cstc2018jcyjA2664) and the China Scholarship Council (No. 201708500037).

## References

- Al Qabany, A., K. Soga, and C. Santamarina. 2012. Factors Affecting Efficiency of Microbially Induced Calcite Precipitation. *Journal of Geotechnical and Geoenvironmental Engineering* 138 (8): 992–1001. doi:10.1061/(ASCE)GT.1943-5606.0000666.
- Ariyanti, D., N. Abyor, and H. Hadi. 2011. An Overview of Biocement Production from Microalgae. *International Journal of Science and Engineering* 2 (2): 30–33. <https://doi.org/10.12777/ijse.2.2.31-33>
- Baveye, P., P. Vandevivere, B. L. Hoyle, P. C. DeLeo, and D. Sanchez De Lozada. 1998. Environmental Impact and Mechanisms of the Biological Clogging of Saturated Soils and Aquifer Materials. *Critical Reviews in Environmental Science and Technology* 28 (2): 123–191. doi:10.1080/10643389891254197.
- DeJong, J. T., M. B. Fritzges, and K. Nüsslein. 2006. Microbially Induced Cementation to Control Sand Response to Undrained Shear. *Journal of Geotechnical and Geoenvironmental Engineering* 132 (11): 1381–1392. doi:10.1061/(ASCE)1090-0241(2006)132:11(1381).
- Erdoğan, S. T., A. M. Forster, P. E. Stutzman, and E. J. Garboczi. 2017. Particle-Based Characterization of Ottawa Sand: Shape, Size, Mineralogy, and Elastic Moduli. *Cement and Concrete Composites* 83: 36–44. doi:10.1016/j.cemconcomp.2017.07.003.

- Harkes, M. P., L. A. van Paassen, J. L. Booster, V. S. Whiffin, and M. C. M. van Loosdrecht. 2010. Fixation and Distribution of Bacterial Activity in Sand to Induce Carbonate Precipitation for Ground Reinforcement. *Ecological Engineering* 36 (2): 112–117. doi:10.1016/j.ecoleng.2009.01.004.
- Hu, J., X. Liu, and P. X. Ma. 2011. Biomineralization and Bone Regeneration. In *Principles of Regenerative Medicine*, ed. A. Atala, R. Lanza, J. A. Thompson, and R. Nerem, 733–745. San Diego, CA: Elsevier/Academic Press.
- Khodadadi Tirkolaei, H., and H. Bilsel. 2017. Estimation on Ureolysis-Based Microbially Induced Calcium Carbonate Precipitation Progress for Geotechnical Applications. *Marine Georesources & Geotechnology* 35 (1): 34–41. doi:10.1080/1064119X.2015.1099062.
- Liang, S., J. Chen, J. Niu, X. Gong, and D. Feng. 2019. Using Recycled Calcium Sources to Solidify Sandy Soil through Microbial Induced Carbonate Precipitation. *Marine Georesources & Geotechnology*, 1–7. doi:10.1080/1064119X.2019.1575939.
- Nouri, A., and A. Sola. 2018. Metal Particle Shape: A Practical Perspective. *Metal Powder Report* 73 (5): 276–282. doi:10.1016/j.mprp.2018.04.001.
- Phillips, A. J., R. Gerlach, E. Lauchnor, A. C. Mitchell, A. B. Cunningham, and L. Spangler. 2013. Engineered Applications of Ureolytic Biomineralization: A Review. *Biofouling* 29 (6): 715. doi:10.1080/08927014.2013.796550.
- Qabany, A. A., and K. Soga. 2013. Effect of Chemical Treatment Used in MICP on Engineering Properties of Cemented Soils. *Géotechnique* 63 (4): 331. doi:10.1680/geot.SIP13.P.022.
- Qian, C.-X., A. Wang, and X. Wang. 2015. Advances of Soil Improvement with Bio-Grouting. *Rock and Soil Mechanics* 6: 1537–1548. doi:10.16285/j.rsm.2015.06.003.
- Rebata-Landa, V. 2007. Microbial Activity in Sediments: Effects on Soil Behavior. PhD diss., Georgia Institute of Technology, Atlanta, GA.
- Song, C., and D. Elsworth. 2018. Strengthening Mylonitized Soft-Coal Reservoirs by Microbial Mineralization. *International Journal of Coal Geology* 200: 166–172. doi:10.1016/j.coal.2018.11.006.
- Sutton, S. 2011. Measurement of Microbial Cells by Optical Density. *Journal of Validation Technology* 17: 46–50. doi:10.1177/002215549904700703
- Tian, Z. F., X. Tang, Z. L. Xiu, and Z. J. Xue. 2019. Effect of Different Biological Solutions on Microbially Induced Carbonate Precipitation and Reinforcement of Sand. *Marine Georesources & Geotechnology*, 1–11. doi:10.1080/1064119X.2019.1595229.
- van Paassen, L. 2009. Biogrout: Ground Improvement by Microbially Induced Carbonate Precipitation, Technology. PhD diss., TU Delft, Delft University of Technology, Delft.
- van Paassen, L. A., C. M. Daza, M. Staal, D. Y. Sorokin, W. van der Zon, and M. C. M. van Loosdrecht. 2010. Potential Soil Reinforcement by Biological Denitrification. *Ecological Engineering* 36 (2): 168–175. doi:10.1016/j.ecoleng.2009.03.026
- Wang, Z., N. Zhang, G. Cai, Y. Jin, N. Ding, and D. Shen. 2017. Review of Ground Improvement Using Microbial Induced Carbonate Precipitation (MICP). *Marine Georesources & Geotechnology* 35 (8): 1135–1146. doi:10.1080/1064119X.2017.1297877.
- Weiner, S., and P. M. Dove 2003. An overview of biomineralization processes and the problem of the vital effect. *Reviews in mineralogy and geochemistry* 54 (1): 1–29. doi:10.2113/0540001.
- Whitehead, K. A., D. Rogers, J. Colligon, C. Wright, and J. Verran. 2006. Use of the Atomic Force Microscope to Determine the Effect of Substratum Surface Topography on the Ease of Bacterial Removal. *Colloids Surfaces B Biointerfaces* 51 (1): 44–53. doi:10.1016/j.colsurfb.2006.05.003.
- Whitehead, K. A., and J. Verran. 2006. The Effect of Surface Topography on the Retention of Microorganisms. *Food and Bioproducts Processing* 84 (4): 253–259. doi:10.1205/fbp06035.
- Wu, J., X. B. Wang, H. F. Wang, and R. J. Zeng. 2017. Microbially Induced Calcium Carbonate Precipitation Driven by Ureolysis to Enhance Oil Recovery. *RSC Advances* 7 (59): 37382–37391. doi:10.1039/C7RA05748B.